Monthly Notices
of the
ROYAL ASTRONOMICAL SOCIETY

MNRAS **510,** 3641–3649 (2022)
Advance Access publication 2021 December 21

https://doi.org/10.1093/mnras/stab3701

Transient quasi-periodic oscillations at γ-rays in the TeV blazar PKS 1510-089

Abhradeep Roy [1]★ Arkadipta Sarkar [1]★ Anshu Chatterjee [1] Alok C. Gupta [2] Varsha Chitnis[1] and P. J. Wiita[3]

[1]*Department of High Energy Physics, Tata Institute of Fundamental Research, Homi Bhabha Road, Mumbai-400005, India*
[2]*Aryabhatta Research Institute of Observational Sciences (ARIES), Manora Peak, Nainital 263002, India*
[3]*Department of Physics, The College of New Jersey, PO Box 7718, Ewing, NJ 08628-0718, USA*

Accepted 2021 December 14. Received 2021 December 13; in original form 2021 November 22

ABSTRACT

We present periodicity search analyses on the γ-ray light curve of the TeV blazar PKS 1510-089 observed by the *Fermi* Large Area Telescope. We report the detection of two transient quasi-periodic oscillations: A 3.6-d QPO during the outburst in 2009 that lasted five cycles (MJD 54906–54923); and a periodicity of 92 d spanning over 650 d from 2018 to 2020 (MJD 58200–58850), which lasted for seven cycles. We employed the Lomb–Scargle periodogram, Weighted Wavelet Z-transform, REDFIT, and the Monte Carlo light-curve simulation techniques to find any periodicity and the corresponding significance. The 3.6-d QPO was detected at a moderate significance of $\sim 3.5\sigma$, while the detection significance of the 92-d QPO was $\sim 7.0\sigma$. We explore a few physical models for such transient QPOs including a binary black hole system, precession of the jet, a non-axisymmetric instability rotating around the central black hole near the innermost stable circular orbit, the presence of quasi-equidistant magnetic islands inside the jet, and a geometric model involving a plasma blob moving helically inside a curved jet.

Key words: radiation mechanisms: non-thermal – galaxies: active – galaxies: individual (PKS 1510-089) – galaxies: jets – gamma rays: galaxies.

1 INTRODUCTION

Active Galactic Nuclei (AGN) are known to exhibit highly variable emission across the electromagnetic spectrum. Radio-loud AGN contain a pair of highly collimated relativistic plasma jets emanating from the central super-massive black hole (SMBH). The jets are powered by the accretion process of dense ionized gases on to the SMBH. Radio-loud AGNs, with jets oriented close to our line of sight, form a sub-class called the blazars (Urry & Padovani 1995). Blazars are classified further into BL Lacertae objects (BL Lacs) and flat spectrum radio quasars (FSRQs) based on the strength of emission lines present in their optical-UV spectra. BL Lac spectra contain very weak and narrow emission lines, whereas FSRQs show broad and strong emission lines. The Doppler-boosted jet radiation dominates the blazar non-thermal emission from radio to very high energy γ-ray wavebands. Various observational studies show that the blazars display flux variability of the order of minutes to years at γ-ray waveband, as observed by the *Fermi*-LAT and ground-based atmospheric Cherenkov telescopes (Aleksić et al. 2011; Shukla et al. 2018).

Although the nature of blazar variability is mostly non-linear, stochastic, and aperiodic (Kushwaha et al. 2017), many studies have claimed detections of strong quasi-periodic oscillations (QPO) in blazar light curves of different electromagnetic wavebands. In accordance to the variability time-scales, the reported QPOs range from a few tens of minutes to hours to days and even years of time-scales (and references therein Raiteri et al. 2001; Liu, Zhao & Wu 2006; Gupta, Srivastava & Wiita 2009; Lachowicz et al. 2009; King et al. 2013; Gupta 2014, 2018; Ackermann et al. 2015; Zhou et al. 2018; Bhatta 2019; Gupta et al. 2019; Sarkar et al. 2020a; Sarkar et al. 2020b). However, most of the QPOs claimed in older studies are marginal detections in that they lasted for only a 2–4 cycles, while their significances were overestimated (Gupta 2014).

Continuous monitoring of blazars by *Fermi*-LAT in the last 12-yr has led to a few recent highly significant γ-ray QPO detections in different blazars, including a ∼34.5-d transient QPO in PKS 2247-131 (Zhou et al. 2018), a ∼71-d transient QPO in B2 1520 + 31 (Gupta et al. 2019), a ∼47-d QPO in 3C 454.3 (Sarkar et al. 2020a), a fast periodicity of ∼7.6 d in CTA 102 during an outburst (Sarkar et al. 2020b), and a periodicity of ∼314 d in OJ 287 (Kushwaha et al. 2020). Although Covino, Sandrinelli & Treves (2019) did the periodogram analysis on the *Fermi*-LAT aperture photometry light curves of 10 blazars and claimed the absence of any global significant periodicity in γ-rays, a more systematic approach to γ-ray QPO detection by Peñil et al. (2020), involving multiple independent techniques applied on about 2300 AGNs, revealed the presence of global periodicities of $>4\sigma$ significance in 11 sources, along with 13 more sources with moderately significant ($3–4\sigma$) QPOs.

According to the leptonic models for jet-dominated blazar emission, the source of the radio through optical-UV photons from blazars is the synchrotron emission by the dense population of ultra-relativistic electrons inside the magnetised jet. External photon fields from the accretion disc, the broad-line region (BLR), and the dusty

★ E-mail: abhradeep.1996@gmail.com (AR); sarkadipta@gmail.com (AS)

torus can enter the jet. Along with the synchrotron photons, these external photons get Compton-upscattered by the same relativistic electron population and produce the high-energy γ-rays, often up to TeV energies. A few recent studies claimed probably related QPOs in optical and γ-rays for several sources, although the significances were low (Sandrinelli et al. 2016a; Sandrinelli, Covino & Treves 2016b). Ackermann et al. (2015) reported a significant ∼2.2-yr periodicity in highly correlated optical and γ-ray light curves of PG 1553 + 113. Several recent studies have reported simultaneous oscillations in both optical and γ-ray light curves of the blazars BL Lac (Sandrinelli et al. 2017), 3C 454.3 (Sarkar et al. 2020a), and CTA 102 (Sarkar et al. 2020b).

PKS 1510-089 (R.A. = 15h 12m 52.2s, Dec. = −09° 06' 21.6") belongs to the FSRQ sub-class of blazars, and it is situated at a cosmological redshift of $z = 0.361$. It is one of the most well-studied blazars and shows high variability across all electromagnetic wavebands (Zacharias 2018). The H.E.S.S. telescope detected PKS 1510-089 in 2010 at TeV energies (H. E. S. S. Collaboration 2013). It exhibits occasional huge multi-wavelength outbursts crossing the daily γ-ray flux level of 10^{-5} photons cm^{-2} s^{-1} (Barnacka et al. 2014; Prince, Majumdar & Gupta 2017; Meyer, Scargle & Blandford 2019), as well as orphan γ-ray flaring episodes (Patel et al. 2021). These correlated multi-wavelength flares can be explained using a shock-in-jet model that indicates the formation of an emission component in the compact core region, resulting in optical and γ-ray flares (Beaklini, Dominici & Abraham 2017). Recently, PKS 1510-089 has been subject to several QPO studies at different wavelengths. Sandrinelli et al. (2016a) carried out QPO searches on about 3000-d long quasi-simultaneous multi-wavelength light curves (MJD 54000–57000) and reported modestly significant periodicities of 115 d ($<3\sigma$) in γ-rays, 206 and 490 d ($\sim3\sigma$) in the optical-R band, and 207 and 474 d ($>3\sigma$) in the IR-K band. Wu et al. (2005) detected periodic deep flux minima of around 1.84 yr in its optical observations of past few years and inferred the presence of a binary black hole system at the centre. Based on 27-yr long UMRAO data of PKS 1510-089 at 4.8, 8, and 14.5 GHz, Fan et al. (2007) claimed a possible ∼12-yr periodicity. The 15-yr long 22 and 37 GHz radio data from 1990 to 2005 revealed two periodicities of 0.9 and 1.8 yr, which agrees well with the deep flux minima periodicity of 1.84 yr and thereby, strengthens the binary black hole assumption (Xie et al. 2008; Zhang et al. 2009; Fu et al. 2014). According to Castignani et al. (2017), QPO analysis of hard X-ray data of PKS 1510-089 taken by RXTE-PCA from 1996 to 2011 reveals no obvious periodicity. The most recent QPO study on radio data of PKS 1510-089 spanning over 38 yr detects quite significant ($>4\sigma$) QPOs of ∼570, ∼800, and ∼1070 d in the 8 GHz and 14.5 GHz light curves (Li et al. 2021).

In this paper, we report the detection of a probable fast γ-ray periodicity of 3.6 d on top of the outburst in 2009 with $>3.5\sigma$ significance and a strong ∼3-month periodicity during a moderate state of activity between 2018 and 2020 with a significance above 7σ. We look for the plausible scenarios among several QPO models proposed in the literature to explain these transient QPOs. We consider that the 3.6-d QPO might have resulted from a hotspot rotating close to the innermost stable circular orbit around the central SMBH, or from enhanced emission from a few quasi-equidistant magnetic islands inside the jet. The source of the 92-d QPO could well be a helical motion of a plasma blob inside a curved jet. We state the *Fermi*-LAT data analysis procedure in Section 2, and describe the QPO finding algorithms in Section 3. Then, we summarize our major results in Section 4. We try to interpret our key results on the basis of various physical models in Section 5 and summarize our conclusions in Section 6.

2 OBSERVATIONS AND DATA ANALYSIS

A detailed recent study on γ-ray periodicity in AGN by Peñil et al. (2020) showed that any long-lived QPO in PKS 1510-089 is not significant ($<3\sigma$). But on visual inspection, the weekly *Fermi*-LAT aperture photometry light curve from MJD 58000 to MJD 59400 seemed to have some periodicity during a long moderate activity state. Moreover, the flare state light curve modelling by Prince et al. (2017) indicated the presence of fast periodicity (∼ days) during the flare between MJD 54890 and MJD 54935.

2.1 *Fermi*-LAT data

We obtained the γ-ray data from the Large Area Telescope (LAT) facility, on-board the *Fermi* observatory. The *Fermi*-LAT is an imaging space-based telescope that detects γ-rays using the pair-production technique within the 30 MeV–1 TeV energy range. LAT has a large angular field of view of about 2.3 sr and covers the entire sky every 3 h (Atwood et al. 2009). We collected the PASS8 (P8R3) processed events' data of PKS 1510-089 between MJD 54890–54935 and MJD 58000–59400 from the *Fermi*-LAT data archive.[1] The PASS8 data provides a significant improvement in the data quality using an improved reconstruction of the entire LAT events (Abdollahi et al. 2020).

2.2 Data REDUCTION

We used the standard software package FERMITOOLS-v2.0.8 recommended by the *Fermi*-LAT collaboration (Fermi Science Support Development Team 2019) and the user-contributed python script ENRICO (Sanchez & Deil 2013). Following the recommendations of the *Fermi*-LAT collaboration,[2] we chose the events belonging to the SOURCE class `(evclass=128, evtype = 3)` within the energy range of 0.1–300 GeV from a circular region of interest (ROI) having a radius of 15°entred at the source PKS 1510-089. To get rid of the γ-ray contribution from the Earth's albedo, we selected the events having zenith angle less than 95° followed by the good time interval selection using the standard filter `'(DATA_QUAL> 0) && (LAT_CONFIG = = 1)'`. We generated an XML file containing the spectral shapes of all the sources lying within ROI + 10° radius around the source location according to the fourth *Fermi*-LAT (4FGL) catalogue, including the γ-ray background emission templates `'gll_iem_v07.fits'` and `'iso_P8R3_SOURCE_V3_v1.txt'` for the Galactic and extra-galactic contributions respectively. We carried out an unbinned maximum-likelihood analysis over the input XML spectral file using the GTLIKE tool to obtain the source spectrum using the instrumental response function `P8R3_SOURCE_V3`. Except for scaling factors, We kept all the spectral parameters free to vary during the optimization process for the sources lying within 5° from PKS 1510-089. The iterative likelihood analysis removed the sources having significance less than 1σ after each fitting pass. As mentioned in the 4FGL catalogue, the final source spectrum was modelled using a log-parabola given as,

$$\frac{\mathrm{d}N}{\mathrm{d}E} = k\left(\frac{E}{E_b}\right)^{-\alpha-\beta\log(E/E_b)}, \quad (1)$$

where α is the spectral index at the break energy (E_b). We kept E_b fixed during the likelihood fitting process.

[1] https://fermi.gsfc.nasa.gov/ssc/data/access/
[2] https://fermi.gsfc.nasa.gov/ssc/data/analysis/

The full 12-yr *Fermi* unfiltered aperture photometry light curve (Fig. 1a) was obtained from the *Fermi* monitoring source list webpage.[3] To extract the γ-ray light curve, we divided the whole epoch in a number of time-bins of our required size and carried out the entire above-mentioned procedure in each time-bin. For the epoch of MJD 54890–54935, we made a light curve with 3-h long bins (Fig. 1b), and for the epoch of MJD 58000–59400, we set the bin size to 7 d (Fig. 1c). For the time-bins where the test-statistics of the flux estimation were less than 16 (i.e. essentially $<4\sigma$ detection significance), we estimated flux upper limits at 95 per cent confidence level using the profile-likelihood method.

3 QPO ANALYSIS METHODS

On visual inspection, the light curves indicated possible quasi-periodic modulations. To estimate the time-period of the modulation and the corresponding significance, we applied four different methods to analyse the light curves: The Generalised Lomb–Scargle periodogram (GLSP), Weighted Wavelet Z-transform (WWZ), REDFIT, and light-curve simulations. These methods follow different approaches to detect periodicities and their corresponding significances in unevenly sampled time series. Although we have used evenly binned *Fermi*-LAT light curves, they became unevenly sampled due to the omission of flux upper-limits in the analysis processes. The details of these methods are discussed below.

3.1 Generalised Lomb–Scargle periodogram

The periodogram is one of the most common methods to find periodicities in light curves, and it gives the power of flux modulations at different frequencies. For an evenly sampled light curve, the square of the modulus of its discrete Fourier transform gives the periodogram. But for irregular sampling, the Lomb–Scargle periodogram (LSP) method iteratively fits sinusoids with different frequencies to the light curve and constructs a periodogram from the goodness of the fit (Lomb 1976; Scargle 1982). In this work, we used the Generalised LSP sub-package of the PYASTRONOMY python package[4] (Czesla et al. 2019). Unlike the classical LSP, the GLSP fits a sinusoid plus a constant to the light curve and takes the errors associated to the measured fluxes into account (Zechmeister & Kürster 2009). This code also provides the significance of a peak in the periodogram in terms of the false alarm probability (FAP) given as,

$$FAP(Pn) = 1 - (1 - prob(P > Pn))^M, \tag{2}$$

where the *FAP* denotes the probability that at least one out of M independent power values in a given frequency band of a white-noise periodogram is larger than or equal to the power threshold, Pn. In this work, a peak in a periodogram was considered to be significant when it crossed the 1 per cent FAP line. The peak position and its corresponding uncertainty were estimated by fitting a Gaussian to the dominant periodogram-peak. GLSP is an effective tool to find persistent periodicities. But it cannot usually detect transient periodicities, as the non-periodic part of the light curve decreases the goodness of GLSP sinusoid fit. Therefore, the power of the transient periodicity is reduced.

3.2 Weighted Wavelet Z-transform

We used the WWZ method to detect transient quasi-periodicities (Foster 1996). The WWZ method convolves a light curve with a time- and frequency-dependent kernel and decomposes the data into time and frequency domains to create a WWZ map. In this work, we used the Morlet kernel (Grossmann & Morlet 1984) having the following functional form,

$$f[\omega(t-\tau)] = \exp\left[\iota\omega(t-\tau) - c\omega^2(t-\tau)^2\right]. \tag{3}$$

Then the WWZ map is given as,

$$W[\omega, \tau; x(t)] = \omega^{1/2} \int x(t) f^*[\omega(t-\tau)]\mathrm{d}t, \tag{4}$$

where f^* is the complex conjugate of the Morlet kernel f, ω is the frequency, and τ is the time-shift. This kernel acts as a windowed discrete Fourier transform having a frequency dependant window size of $\exp[-c\omega^2(t-\tau)^2]$. The WWZ map has the advantage of being able to detect both any dominant periodicities and the time spans of their persistence.

3.3 REDFIT

The REDFIT[5] software calculates the bias-corrected power-spectrum of a time series and provides the significance of the peaks in the spectrum (Schulz & Mudelsee 2002). REDFIT fits the light curve with a first-order autoregressive process (AR1) to estimate the underlying red-noise spectrum, which is the characteristic of variable γ-ray emission from blazars (Covino, Sandrinelli & Treves 2018). The autoregressive (AR) models assume that the present observation in a time series is related to the past observations. Thus, large fluctuations in the light curve become less likely (Robinson 1977). A discrete AR1 process $\mathscr{F}$ for times t_i ($i = 1, 2,..., N$) with uneven spacing is given as,

$$\begin{aligned} \mathscr{F}(t_i) &= \theta_i \mathscr{F}(t_{i-1}) + \epsilon(t_i), \\ \theta_i &= \exp((t_{i-1} - t_i)/\tau), \end{aligned} \tag{5}$$

where τ is the characteristic time-scale and ϵ denotes white-noise with zero mean. The power-spectrum of an AR1 model has the following analytical form (Percival & Walden 1993),

$$G_{rr}(f_j) = G_0 \frac{1-\theta^2}{1 - 2\theta\cos(\pi f_j / f_{Nyq}) + \theta^2}, \tag{6}$$

where f_j denotes the discrete frequency up to the Nyquist frequency (f_{Nyq}) and G_0 is the average spectral amplitude. The 'average autoregression coefficient' (θ) is related to the arithmetic mean of the sampling intervals $\Delta t = (t_N - t_1)/(N-1)$ as, $\theta = \exp(-\Delta t/\tau)$, while the τ comes from the Welch-overlapped-segment-averaging (WOSA, Welch 1967) of the LSP.REDFIT estimates the significance of the peaks in the power-spectrum using FAP level up to the minimum of 1 per cent.

3.4 Light-curve simulation

Another way to estimate the peak significance in a periodogram is to simulate light curves using a Monte Carlo method, following the power spectral density (PSD) and the flux distribution (PDF) of the original light curve (Emmanoulopoulos, McHardy & Papadakis

[3] https://fermi.gsfc.nasa.gov/ssc/data/access/lat/msl_lc
[4] https://github.com/sczesla/PyAstronomy
[5] https://www.manfredmudelsee.com/soft/redfit/index.htm

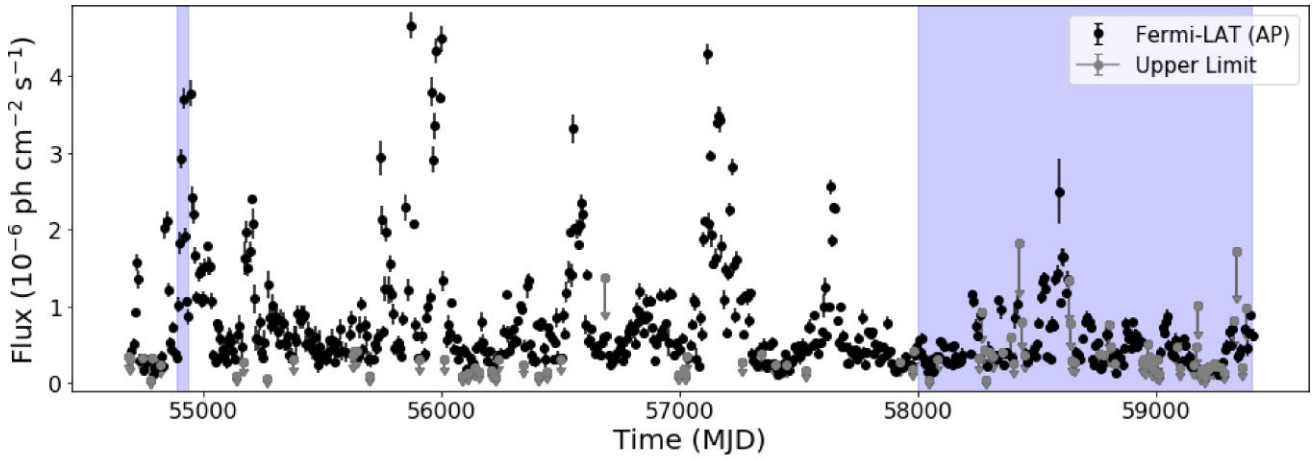

(a)

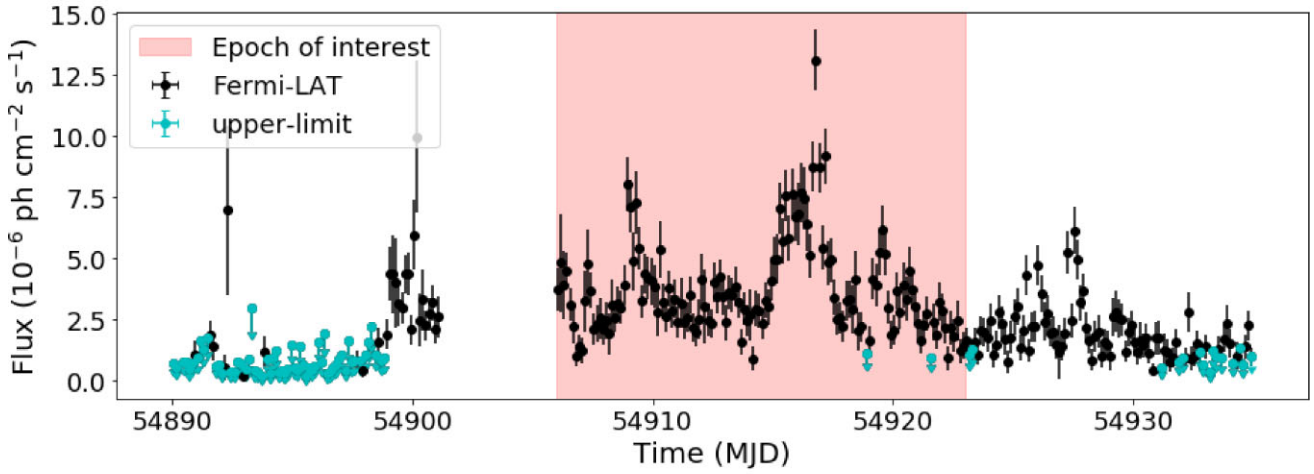

(b)

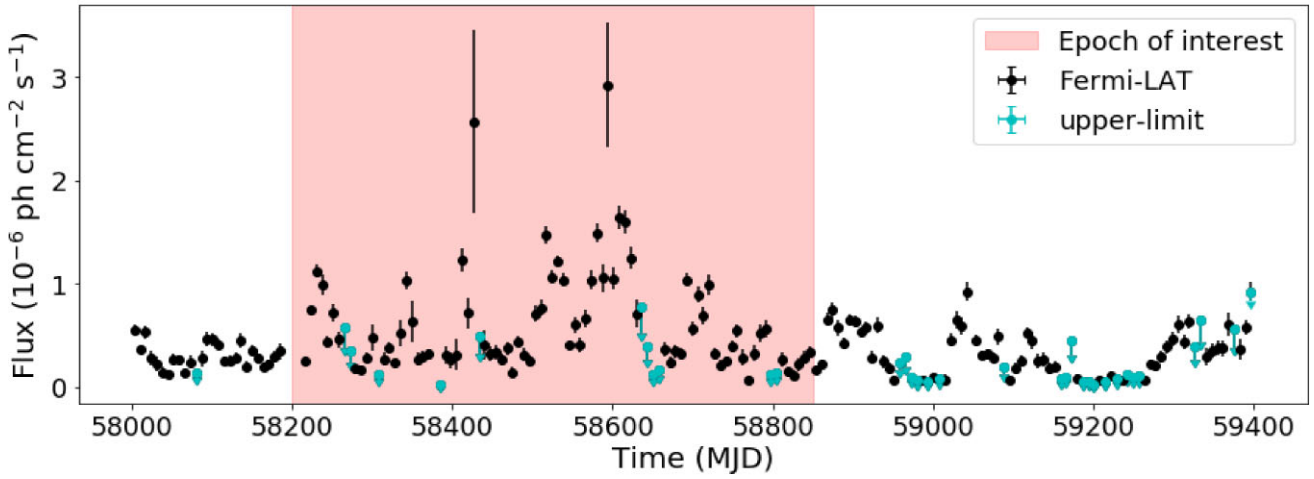

(c)

Figure 1. Top: *Fermi* 12-yr weekly aperture photometry light curve. The blue shaded regions are the epochs where QPO analyses were carried out (i.e. MJD 54890–54935 and MJD 58000–59400). Middle: *Fermi* 3-h-binned light curve within MJD 54890–54935. The pink shaded region is the epoch MJD 54906–54923 (EP1) where the final QPO analyses were carried out. Bottom: *Fermi* 7-d-binned light curve within MJD 58000–59400. The pink shaded region is the epoch MJD 58200–58850 (EP2) where the final QPO analyses were carried out.

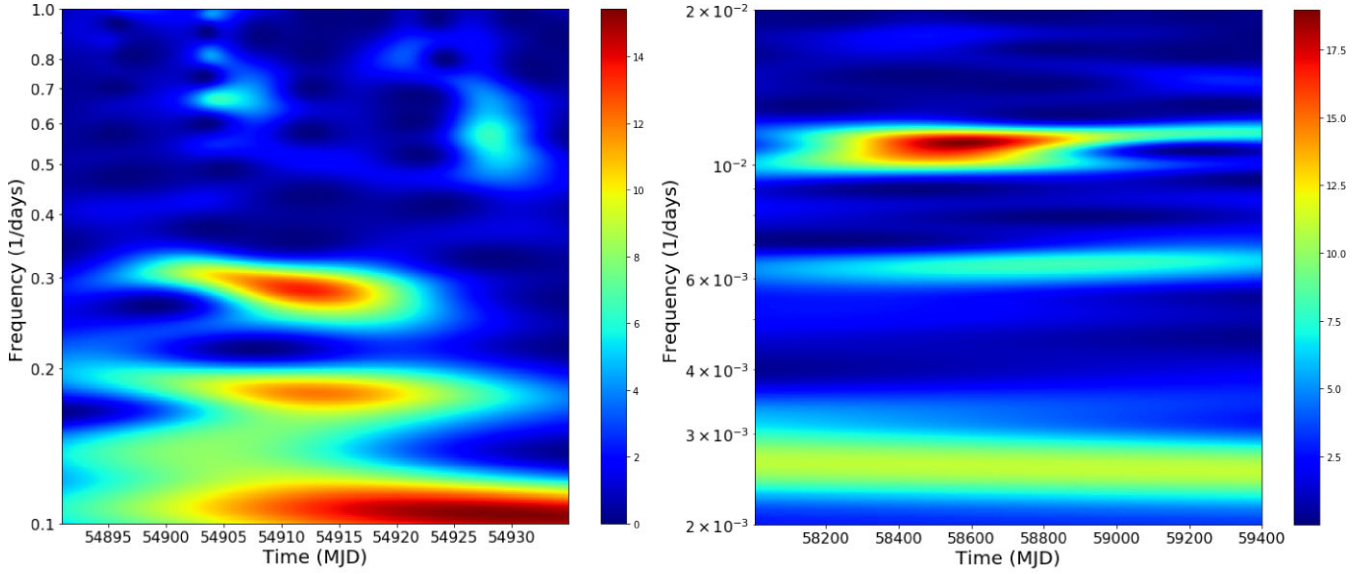

Figure 2. Left: WWZ map of PKS 1510-089 γ-ray light curve in the interval of MJD 54890–54935. The bright yellowish red patch around the frequency of 0.3 d^{-1} indicates the possible presence of a QPO in the interval of MJD 54900–54923. Right: WWZ map of PKS 1510-089 γ-ray light curve in the interval of MJD 58000–59400. The bright red patch indicates a probable QPO in the interval of MJD 58200–58850.

2013). Simple power-laws ($P \propto \nu^{-\alpha}$) give reasonably good approximations of the underlying red-noise PSDs of blazar light curves (Vaughan 2005). Hence, we used a power-law and a lognormal model to respectively fit the PSD and PDF of the original light curve. The lognormal model for PDF has the form,

$$PDF(x) = \frac{1}{x\sigma\sqrt{2\pi}} \exp\left[-\frac{(\ln x - \mu)^2}{2\sigma^2}\right]. \quad (7)$$

Then, we simulated 2000 light curves with the fitted PSD and PDF models as inputs using the DELIGHTCURVESIMULATION[6] code (Connolly 2016). The mean and standard deviation of the simulated light curve GLSP at each frequency allowed us to estimate the significance of the dominant periodicities.

4 RESULTS

Fig. 1a shows the epochs on the weekly *Fermi*-LAT full aperture photometry light curve that were initially considered for QPO analysis. But after analysing the *Fermi*-LAT data, we selected two sub-intervals (Figs 1b and c) to carry on detailed QPO analysis: MJD 54906–54923 (EP1) and MJD 58200–58850 (EP2).

4.1 EP1: 2009 March 16–2009 April 2 (MJD 54906–54923)

From Fig. 2a, it is evident that there is a QPO in MJD 54900–54923 around the frequency of 0.3 d^{-1}. But in Fig. 1b, it can be clearly seen that there is a big gap in the data and in addition, the available flux points are mostly upper limits during MJD 54890–54906. So, we avoided these intervals and carried out our QPO analyses in EP1 (MJD 54906–54923).

Fig. 3a shows the WWZ map of PKS 1510-089 during EP1. The strong horizontal red patch denoting the 3.6-d QPO spans the entire 18-d EP1 light curve, indicating the presence of 5 cycles. The time-averaged WWZ plot indicates a QPO of 3.6 d with 3.5σ significance. Fig. 3b shows the power-spectrum and the corresponding peak significance obtained using REDFIT. It indicates a QPO of ∼3.7 d, crossing the 5 per cent FAP level. Fig. 3c represents the lognormal fitted flux distribution in this epoch. Fig. 3 shows the LSP of PKS 1510-089 γ-ray light curve during EP1 and the result of significance check using our light-curve simulation. The dominant periodicity of $3.63^{+0.07}_{-0.07}$ d crosses the 0.01 per cent FAP level. We note that this FAP significance estimation only holds for Gaussian random noise, whereas blazars show red-noise type variability. However, the light-curve simulation, which does not rely on that noise assumption, indicates that the QPO of 3.6 d has a significance of 3.5σ.

In recent studies (Kushwaha et al. 2020; Peñil et al. 2020; Sarkar et al. 2020a; Sarkar et al. 2020b), the reported blazar QPOs generally have >3σ significance and cross the REDFIT FAP level of 1 per cent. In this case, the QPO spans only 18 d, and the apparent periodicity is very fast (∼3.6 d) which should be the reason for low significance in the REDFIT output. But from the light-curve simulation, we find a ∼3.5σ significance, which makes the QPO sufficiently significant to be reported. The QPO peak significances remained the same when we applied the same analysis procedures on light curves in EP1 with different bin-sizes, such as 4 or 5 h.

4.2 EP2: 23 March 2018–2 January 2020 (MJD 58200–58850)

Fig. 1c shows the 7-d-binned *Fermi*-LAT light curve between MJD 58000 and MJD 59400. Although the GLSP did not reveal any significant dominant QPO in this interval, the WWZ map showed a bright red patch with a span of ∼650 d from MJD 58200 to MJD 58850 (Fig. 2b). This led to the selection of EP2 (MJD 58200–58850) for detailed analysis.

Fig. 4a shows the WWZ map of PKS 1510-089 during EP2. The strong horizontal red patch, spanning all the 650-d EP2 light curve, denotes a strong 92-d QPO, indicating the presence of 7 cycles. The time-averaged WWZ also show a QPO of 92 d, with

[6]https://github.com/samconnolly/DELightcurveSimulation

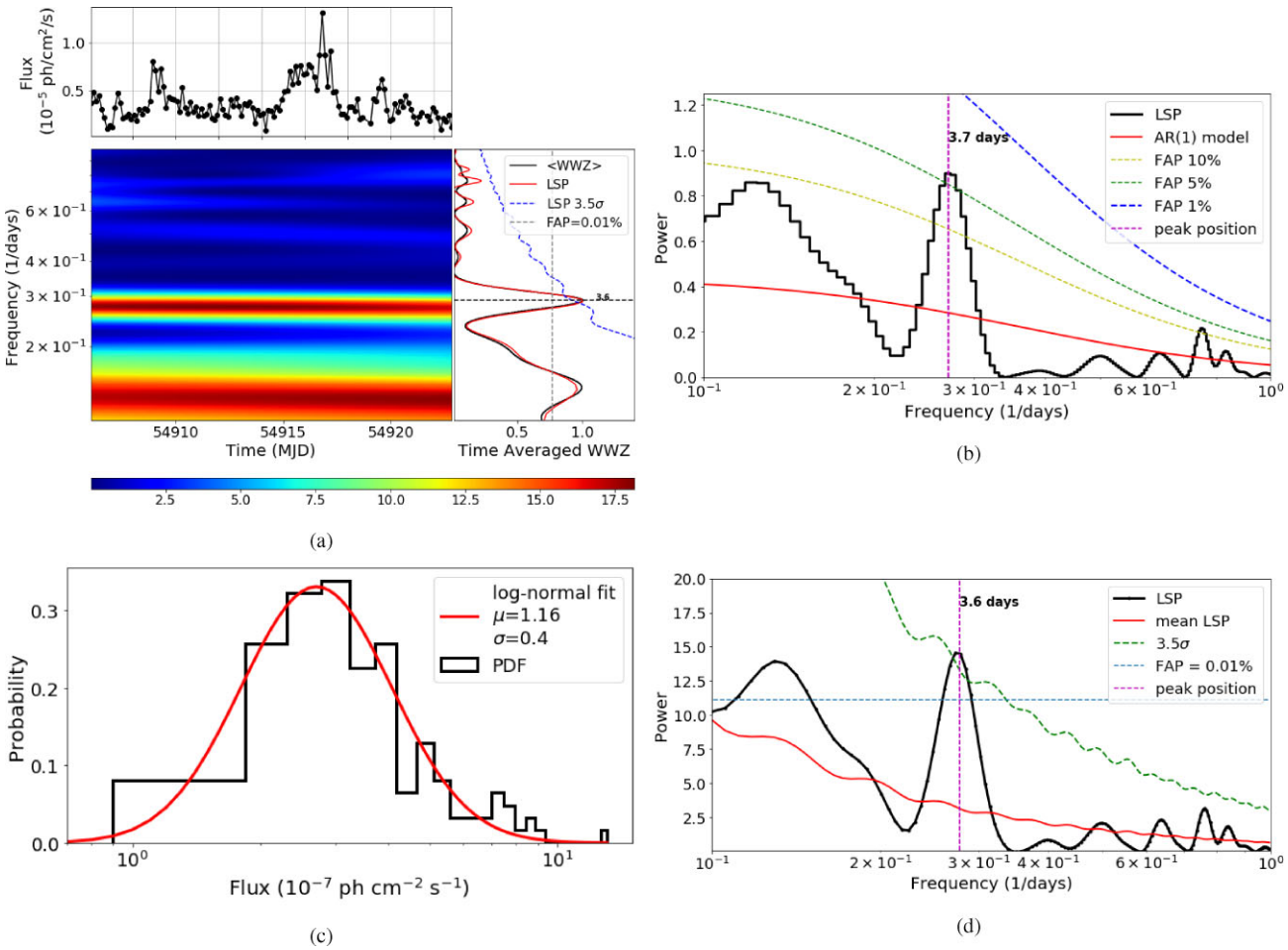

Figure 3. *QPO analysis in EP1 (MJD 54906–54923):* Upper-left: WWZ map of PKS 1510-089 γ-ray light curve during EP1. On the upper-left sub-panel, the light curve is shown; the lower left panel shows the WWZ map; the lower-right sub-panel shows the time-averaged WWZ (black) as well as the LSP (red). The blue-dashed line represents the 3.5σ significance line against the power-law red-noise spectrum and the red band on the WWZ map indicates a strong periodicity of ∼3.6 d. Upper-right: Power-spectrum of PKS 1510-089 γ-ray light curve using REDFIT during EP1. The black line represents the power-spectrum, the red line is the theoretical AR1 spectrum, and the yellow, green, and blue-dashed lines represent FAP levels of 10, 5, and 1 per cent, respectively. A strong periodicity of ∼3.7 d crosses the 5 per cent FAP level. Lower-left: Flux distribution of the PKS 1510-089 γ-ray light curve (PDF in black) fitted with a lognormal model (red) that is used as an input in light-curve simulation. Lower-right: Result of light-curve simulation of the PKS 1510-089 γ-ray light curve during EP1. The black line represents the LSP of the original light curve and the red line is the mean LSP of the simulated light curves. The dominant period of ∼3.6 d crosses the 0.01 per cent FAP level (cyan-dashed line) and the 3.5σ significance curve (green-dashed curve).

almost 7.0σ significance. Fig. 4b shows the power-spectrum and the corresponding peak significance obtained using REDFIT. It indicates a QPO of ∼92 d, crossing the 1 per cent FAP level. Fig. 4c represent the lognormal fitted flux distribution during EP2. Fig. 4d shows the LSP of PKS 1510-089 γ-ray light curve during EP2 and the significance check of the observed QPO using light-curve simulation. The dominant periodicity of $91.5^{+1.2}_{-1.2}$ d crosses the 0.2 per cent FAP level, if one considers an underlying Gaussian-type noise. Light-curve simulation shows that the QPO of 92 d seems to have a significance of $>6\sigma$. The 92-d peak touches the blue-dashed 7.0σ significance line. Thus, all the applied tools indicate this 92-d QPO to be highly significant. We have also checked that our key results remain the same when light curves produced when we employed different bin-sizes of 3 or 5 d during EP2.

5 DISCUSSION

We obtained γ-ray data from the *Fermi*-LAT archive and analysed then to generate the light curves in two different epochs: EP1 (MJD 54906–54923) and EP2 (MJD 58200–58850). We employed LSP, WWZ, and REDFIT methods to detect significant transient periodicities in the light curves. We generated 2000 light curves in each epoch using Monte Carlo simulation to account for the underlying red-noise spectrum while estimating the QPO significances. All of these methods revealed two highly probable transient QPOs: (1) A fast QPO of 3.6 d in EP1 and; (2) a 92-d QPO in EP2.

Due to lack of good coverage of optical observations during the selected epochs, it was not possible to employ QPO analysis tools on the available optical data. In case of an FSRQ, both synchrotron emission from the jet and thermal emission from the accretion disc contribute to the optical-UV emission. The γ-ray emission is dominated by the inverse-Compton scattering of seed photons by the charged particle population inside the jet responsible for the synchrotron emission. Thus, simultaneous optical and γ-ray QPO can lead to strong inferences about possible reasons behind such phenomena and the underlying disc-jet connection. Only having γ-ray data here, it is quite hard to conclusively investigate the probable physical reasons behind such

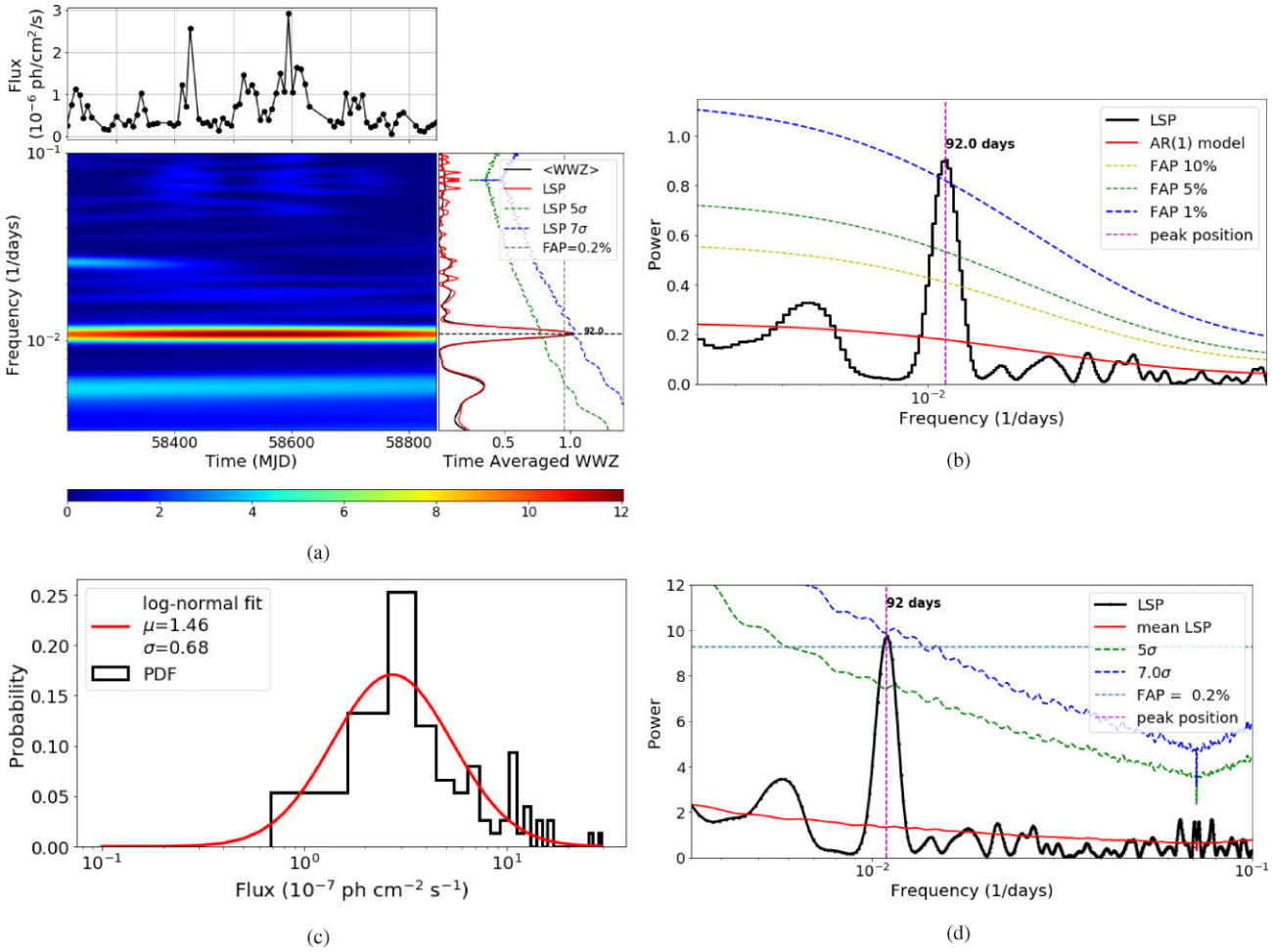

Figure 4. *QPO analysis in EP2 (MJD 58200–58850):* Upper-left: WWZ map of the PKS 1510-089 γ-ray light curve during EP2. On the upper-left sub-panel, the light curve is shown, the lower left sub-panel displays the WWZ map, and the lower-right sub-panel shows the time-averaged WWZ power (black) on top of the LSP (red). The green- and blue-dashed curves represent the 5.0 and 7.0σ significance, respectively against the power-law red-noise spectrum and the red band on the WWZ map indicates a strong periodicity of ∼92 d. Upper-right: Power-spectrum of PKS 1510-089 γ-ray light curve using REDFIT during EP2. The black line represents the power-spectrum, the red line is the theoretical AR1 spectrum, and the yellow, green, and blue-dashed lines represent FAP level of 10, 5, and 1 per cent, respectively. A strong periodicity of ∼92 d crosses the 1 per cent FAP level. Lower-left: PDF of the flux distribution of PKS 1510-089 γ-ray light curve (black) fitted with a lognormal model (red) that is used as an input in the light-curve simulations. Lower-right: Result of light-curve simulations of PKS 1510-089 γ-ray light curve during EP2. The black line represents the LSP of the original light curve, and the red line is the mean LSP of the simulated light curves. The dominant period of ∼92 d crosses the 0.2 per cent FAP level (cyan-dashed line) and the 5σ significance level (green-dashed curve) and nearly touches a significance of 7.0σ (blue-dashed curve).

periodicities. Still, the γ-ray QPO time-scale and persistence can lead to a few insights about the jet structure or emission processes.

Earlier studies have proposed several possible models, such as supermassive binary black hole systems (Valtonen et al. 2008; Villforth et al. 2010; Ackermann et al. 2015; Li et al. 2021), persistent jet precession model (Romero et al. 2000; Rieger 2004; Liska et al. 2018), and Lense–Thirring precession of accretion discs (Stella & Vietri 1998; Liska et al. 2018) to explain the long-term quasi-periodicities in different blazar's emissions. Although PKS 1510-089 is a candidate to contain a binary black hole system at the centre (Wu et al. 2005; Li, Fan & Yuan 2007), all these models exhibit persistent QPOs with at least year-long periods. So, we can probably discard these models as an explanation for the QPOs discussed here.

Optical QPOs with tens of days period can be explained by hot-spots rotating at or near the innermost stable circular orbit (ISCO) around the central SMBH (Zhang & Bao 1991; Gupta et al. 2009). In this case, the rotation of the hotspot will modulate the seed photon field of the external inverse-Compton scattering inside the jet, causing a modulation in the γ-ray emission. The γ-ray emission from blazar jet is Doppler boosted and should have a faster quasi-periodicity (∼days) in this model. Thus, rotation of a hot spot near the ISCO could be a possible scenario behind the ∼3.6-d QPO on top of the flare during EP1. Availability of an optical counterpart of this short QPO could actually emphasise the applicability of this model in EP1. Assuming that the QPO is related to orbital rotation of a hotspot, presence of a spiral shock, or any other non-axisymmetric instabilities close to the ISCO, we can estimate the central SMBH mass using an expression given by Gupta et al. (2009),

$$\frac{M_{\rm BH}}{\rm M_\odot} = \frac{3.23 \times 10^4 P}{(r^{3/2} + a)(1+z)}, \tag{8}$$

where P is the QPO period in seconds, z is the cosmological redshift of the source ($z = 0.361$ for PKS 1510-089), r is the radius of ISCO in units of $GM_{\rm BH}/c^2$, and a is the SMBH spin parameter.

For a Schwarzschild black hole, $r = 6.0$ and $a = 0$, and for a maximally rotating Kerr black hole, $r = 1.2$ and $a = 0.9982$. Using the period of ∼3.6 d, the estimated mass of a Schwarzschild BH is $\sim 5.0 \times 10^8\,{\rm M}_\odot$, and the mass of a maximally rotating Kerr BH is $\sim 3.2 \times 10^9\,{\rm M}_\odot$. While using the period of 92 d, we get the mass estimate of Schwarzschild BH to be $\sim 1.2 \times 10^{10}\,{\rm M}_\odot$, and that of a Kerr BH to be $\sim 8.2 \times 10^{10}\,{\rm M}_\odot$. There are various methods to estimate the mass of the central SMBH. Gu, Cao & Jiang (2001) used the data of the H_β line width and the optical continuum luminosity and reported a mass of $\sim 1.3 \times 10^9\,{\rm M}_\odot$ for the central SMBH of PKS 1510-089. The reverberation mapping technique is one of the most accurate methods to estimate the mass of a primary black hole. Rakshit (2020) reported a mass of $\sim 5.71 \times 10^7\,{\rm M}_\odot$ for the SMBH of PKS 1510-089 using a stereoscopic reverberation mapping technique. Xie et al. (2005) used reverberation mapping and short-time-scale optical variability to estimate the SMBH mass to be $\sim 2.0 \times 10^8$ and $\sim 1.6 \times 10^8\,{\rm M}_\odot$, respectively. The masses estimated using the 92-d QPO are much higher, thereby essentially excluding the possibility that disc instabilities directly yield it. But the masses estimated using the 3.6-d QPO are comparable to the SMBH mass estimated by Gu et al. (2001). If this is the case, it favours the presence of a non-maximally rotating SMBH at the centre. However, this rotating hot-spot scenario suffers a major disadvantage in explaining blazar fluctuations. Blazar discs have almost face-on orientation with respect to the observer, so the motion of the rotating hotspot should be almost azimuthally symmetric, which implies that this situation is unlikely to generate enough flux variability. Rotating hotspots are more likely to generate QPOs if the observer's line of sight is close to the plane of the accretion disc (Rani, Wiita & Gupta 2009).

Another interesting model that might explain fast quasi-periodicity in the jet emission involves magnetic reconnection events in almost equidistant magnetic islands inside the jet (Huang et al. 2013). These equispaced magnetic islands periodically enhance the flux, thereby producing a rapid transient QPO. Shukla et al. (2018) used such a magnetic reconnection process to model the extremely fast variability (∼5 minutes) in the FSRQ CTA 102 during its outburst in 2016. This model does appear to be capable of producing the 3.6-d QPO in γ-rays for PKS 1510-089, and suffers no obvious difficulties.

We can also attempt to attribute both the 3.6-d and 92-d QPO of PKS 1510-089 to a very reasonable model that involves a plasma blob moving helically down the jet (Mohan & Mangalam 2015; Sobacchi, Sormani & Stamerra 2016; Sarkar et al. 2020a). For the simplest leptonic one-zone model (where the bulk of the synchrotron and inverse-Compton emission comes from a single region), such a plasma blob contains higher particle and magnetic energy densities and is responsible for occasional enhanced emission from blazars. Due to the postulated helical motion of the blob, the viewing angle of the blob with respect to our line of sight ($\theta_{\rm obs}$) changes periodically with time as,

$$\cos\theta_{\rm obs}(t) = \sin\phi\sin\psi\cos(2\pi t/P_{\rm obs}) + \cos\phi\cos\psi, \quad (9)$$

where ϕ is the pitch angle of the helical path, ψ is the angle of the jet axis with respect to our line of sight, and $P_{\rm obs}$ is the observed periodicity in the light curve (Sobacchi et al. 2016; Zhou et al. 2018). The Doppler factor (δ) varies with the viewing angle as $\delta = 1/[\Gamma(1 - \beta\cos\theta_{\rm obs})]$, where $\Gamma = 1/\sqrt{1-\beta^2}$ is the bulk Lorentz factor of the blob motion with $\beta = v_{\rm jet}/c$. Then, the periodicity in the blob rest frame is given as,

$$P_{\rm rf} = \frac{P_{\rm obs}}{1 - \beta\cos\psi\cos\phi}. \quad (10)$$

This model can naturally explain the transient nature of any periodicities as the QPO starts when the blob is injected into the jet and lasts until the blob dissipates. One limitation of this model is that it can only explain a QPO having almost constant amplitude. It is evident from Figs 3a and 4 a that both the QPOs in EP1 and EP2 have varying amplitudes. We note that Sarkar et al. (2020a) used a curved jet scenario to model a transient QPO with varying amplitude in 3C 454.3. In this model, the angle between the jet axis and our line of sight (ψ) becomes time-dependent ($\psi(t)$). We find that the 'blob moving helically in a curved jet' model might be able to explain them both. Assuming $\phi \simeq 2^\circ$ (Zhou et al. 2018), $\langle\psi\rangle = 2^\circ.2$, $\Gamma = 20.0$ (Roy et al. 2021), and $P_{\rm obs} = 3.6$ d, the periodicity in the blob rest-frame is $P_{\rm rf} \simeq 3.8$ yr. The blob traverses about a distance $D = c\beta P_{\rm rf}\cos\phi \simeq 1.16$ pc down the jet during one period. But only a very high-jet curvature can explain the rapid changes in QPO amplitudes in EP1. However, the presence of high curvature within a few parsecs is highly unlikely in an extremely long, well-collimated, and powerful FSRQ jet. On the other hand, for $P_{\rm obs} = 92$ d, the periodicity in the blob rest-frame is $P_{\rm rf} \simeq 97.1$ yr. The blob travels ∼30 pc during one period, i.e. it travels ∼200 pc during EP2. Fig. 4a shows a slow increasing trend in the first 5 cycles and then a faster attenuation in the QPO amplitudes. This situation can be explained with a much lower curvature in the jet, which is physically more likely. Thus, we tentatively conclude that the 3.6-d QPO probably resulted from flux enhancements by magnetic reconnection events at quasi-equispaced magnetic islands, while most probably the origin of the 92-d QPO is a plasma blob moving helically inside a curved jet.

6 CONCLUSIONS

In this work, we report two transient QPOs in γ-rays exhibited by the TeV blazar PKS 1510-089. We employed several standard tools, such as Lomb–Scargle periodogram, REDFIT, WWZ, and light-curve simulation on the *Fermi*-LAT light curve to detect the significant periodicities. Our key results are as follows:

(i) PKS 1510-089 showed a fast periodicity of ∼3.6 d during a flare in 2009, from MJD 54906 to MJD 54923. It lasted for only 18 d. Light-curve simulation indicates the significance of this QPO to be $\sim 3.5\sigma$ against the underlying red-noise spectrum. To our knowledge, this is the shortest period QPO so far reported in the γ-ray emission of a blazar.

(ii) Multiple QPO analyses show the presence of a QPO around 92 d in the recent *Fermi*-LAT observations that lasted for about 650 d from 2018 to 2020 (MJD 58200–58850). From light-curve simulation, it seems that this periodicity has a significance of about 7σ, and would be the most significant blazar QPO ever reported.

ACKNOWLEDGEMENTS

We would like to thank the anonymous referee whose suggestions have helped us to improve our results and to gain new insights. This research has made use of the *Fermi*-LAT data, obtained from the Fermi Science Support Center, provided by NASA's Goddard Space Flight Center (GSFC). The *Fermi-LAT* Collaboration acknowledges generous on-going support from a number of agencies and institutes that have supported both the development and the operation of the LAT as well as scientific data analysis. These include the National

Aeronautics and Space Administration and the Department of Energy in the USA, the Commissariat l' Energie Atomique and the Centre National de la Recherche Scientifique/Institut National de Physique Nucléaire et de Physique des Particules in France, the Agenzia Spaziale Italiana and the Istituto Nazionale di Fisica Nucleare in Italy, the Ministry of Education, Culture, Sports, Science, and Technology (MEXT), High Energy Accelerator Research Organization (KEK) and Japan Aerospace Exploration Agency (JAXA) in Japan, and the KÀ. Wallenberg Foundation, the Swedish Research Council and the Swedish National Space Board in Sweden. Additional support for science analysis during the operations phase is gratefully acknowledged from the Istituto Nazionale di Astrofisica in Italy and the Centre National d' Études Spatiales in France. The data and analysis software were obtained from NASA's High-Energy Astrophysics Science Archive Research Center (HEASARC), a service of GSFC. We used a community-developed Python package named ENRICO to make *Fermi*-LAT data analysis easier (Sanchez & Deil 2013). Finally, We acknowledge the support of the Department of Atomic Energy, Government of India, under project identification number RTI 4002.

DATA AVAILABILITY

(i) The *Fermi*-LAT data used in this article are available in the LAT data server at https://fermi.gsfc.nasa.gov/ssc/data/access/.

(ii) The *Fermi*-LAT data analysis software is available at https://fermi.gsfc.nasa.gov/ssc/data/analysis/software/.

(iii) We agree to share data derived in this article on reasonable request to the corresponding author.

REFERENCES

Abdollahi S. et al., 2020, ApJS, 247, 33
Ackermann M. et al., 2015, ApJ, 813, L41
Aleksić J. et al., 2011, ApJ, 730, L8
Atwood W. B. et al., 2009, ApJ, 697, 1071
Barnacka A., Moderski R., Behera B., Brun P., Wagner S., 2014, A&A, 567, A113
Beaklini P. P. B., Dominici T. P., Abraham Z., 2017, A&A, 606, A87
Bhatta G., 2019, MNRAS, 487, 3990
Castignani G. et al., 2017, A&A, 601, A30
Connolly S. D., 2016, DELightcurveSimulation: Light curve simulation code, preprint (ascl:1602.012)
Covino S., Sandrinelli A., Treves A., 2018, MNRAS, 482, 1270
Covino S., Sandrinelli A., Treves A., 2019, MNRAS, 482, 1270
Czesla S., Schröter S., Schneider C. P., Huber K. F., Pfeifer F., Andreasen D. T., Zechmeister M., 2019, PyA: Python astronomy-related packages, preprint (ascl:1906.010)
Emmanoulopoulos D., McHardy I. M., Papadakis I. E., 2013, MNRAS, 433, 907
Fan J. H. et al., 2007, A&A, 462, 547
Fermi Science Support Development Team, 2019, Fermitools: Fermi Science Tools, preprint (ascl:1905.011)
Foster G., 1996, AJ, 112, 1709
Fu J. P., Zhang H. J., Zhang X., Xiong D. R., Guo F., 2014, Acta Astron. Sin., 55, 1
Grossmann A., Morlet J., 1984, SIAM J. Math. Anal., 15, 723
Gu M., Cao X., Jiang D., 2001, MNRAS, 327, 1111
Gupta A. C., 2014, J. Astrophys. Astron., 35, 307
Gupta A., 2018, Galaxies, 6, 1
Gupta A. C., Srivastava A. K., Wiita P. J., 2009, ApJ, 690, 216
Gupta A. C., Tripathi A., Wiita P. J., Kushwaha P., Zhang Z., Bambi C., 2019, MNRAS, 484, 5785
H. E. S. S. Collaboration, 2013, A&A, 554, A107
Huang C.-Y., Wang D.-X., Wang J.-Z., Wang Z.-Y., 2013, RAA, 13, 705
King O. G. et al., 2013, MNRAS, 436, L114
Kushwaha P., Sinha A., Misra R., Singh K. P., de Gouveia Dal Pino E. M., 2017, ApJ, 849, 138
Kushwaha P., Sarkar A., Gupta A. C., Tripathi A., Wiita P. J., 2020, MNRAS, 499, 653
Lachowicz P., Gupta A. C., Gaur H., Wiita P. J., 2009, A&A, 506, L17
Li J., Fan J.-H., Yuan Y.-H., 2007, Chin. Phys., 16, 876
Li X.-P., Zhao L., Yan Y., Wang L.-S., Yang H.-T., Cai Y., Luo Y.-H., 2021, J. Astrophys. Astron., 42, 92
Liska M., Hesp C., Tchekhovskoy A., Ingram A., van der Klis M., Markoff S., 2018, MNRAS, 474, L81
Liu F. K., Zhao G., Wu X.-B., 2006, ApJ, 650, 749
Lomb N. R., 1976, Astrophys. Space Sci., 39, 447
Meyer M., Scargle J. D., Blandford R. D., 2019, ApJ, 877, 39
Mohan P., Mangalam A., 2015, ApJ, 805, 91
Patel S. R., Bose D., Gupta N., Zuberi M., 2021, JHEAp, 29, 31
Peñil P. et al., 2020, ApJ, 896, 134
Percival D. B., Walden A. T., 1993, Spectral Analysis for Physical Applications. Cambridge Univ. Press, Cambridge
Prince R., Majumdar P., Gupta N., 2017, ApJ, 844, 62
Raiteri C. M. et al., 2001, A&A, 377, 396
Rakshit S., 2020, A&A, 642, A59
Rani B., Wiita P. J., Gupta A. C., 2009, ApJ, 696, 2170
Rieger F. M., 2004, ApJ, 615, L5
Robinson P. M., 1977, Stoch. Process Their Appl, 6, 9
Romero G. E., Chajet L., Abraham Z., Fan J. H., 2000, A&A, 360, 57
Roy A., Patel S. R., Sarkar A., Chatterjee A., Chitnis V. R., 2021, MNRAS, 504, 1103
Sanchez D. A., Deil C., 2013, preprint (arXiv:1307.4534)
Sandrinelli A., Covino S., Dotti M., Treves A., 2016a, AJ, 151, 54
Sandrinelli A., Covino S., Treves A., 2016b, ApJ, 820, 20
Sandrinelli A. et al., 2017, A&A, 600, A132
Sarkar A., Gupta A. C., Chitnis V. R., Wiita P. J., 2020a, MNRAS, 501, 50
Sarkar A., Kushwaha P., Gupta A. C., Chitnis V. R., Wiita P. J., 2020b, A&A, 642, A129
Scargle J. D., 1982, ApJ, 263, 835
Schulz M., Mudelsee M., 2002, Computers & Geosciences, 28, 421
Shukla A. et al., 2018, ApJ, 854, L26
Sobacchi E., Sormani M. C., Stamerra A., 2016, MNRAS, 465, 161
Stella L., Vietri M., 1998, ApJ, 492, L59
Urry C. M., Padovani P., 1995, PASP, 107, 803
Valtonen M. J. et al., 2008, Nature, 452, 851
Vaughan S., 2005, A&A, 431, 391
Villforth C. et al., 2010, MNRAS, 402, 2087
Welch P., 1967, IEEE Trans. Audio Electroacoust., 15, 70
Wu J., Zhou X., Peng B., Ma J., Jiang Z., Chen J., 2005, MNRAS, 361, 155
Xie G. Z., Liu H. T., Cha G. W., Zhou S. B., Ma L., Xie Z. H., Chen L. E., 2005, AJ, 130, 2506
Xie G. Z., Yi T. F., Li H. Z., Zhou S. B., Chen L. E., 2008, AJ, 135, 2212
Zacharias M., 2018, preprint (arXiv:1903.02274)
Zechmeister M., Kürster M., 2009, A&A, 496, 577
Zhang H., Zhao G., Zhang X., Dong F., Xie Z., Yi T., Zheng Y., Yu Y., 2009, Sci. China Phys. Mech, 52, 1442
Zhang X. H., Bao G., 1991, A&A, 246, 21
Zhou J., Wang Z., Chen L., Wiita P. J., Vadakkumthani J., Morrell N., Zhang P., Zhang J., 2018, Nat. Commun., 9, 4599

This paper has been typeset from a TEX/LATEX file prepared by the author.